

# A model for investigating the influence of road surface texture and tyre tread pattern on rolling resistance<sup>☆</sup>

Carsten Hoever<sup>a,\*</sup>, Wolfgang Kropp<sup>a</sup>

<sup>a</sup>*Division of Applied Acoustics, Chalmers University of Technology, SE-41296 Göteborg, Sweden*

---

## Abstract

The reduction of rolling resistance is essential for a more environmentally friendly road transportation sector. Both tyre and road design can be utilised to reduce rolling resistance. In both cases a reliable simulation tool is needed which is able to quantify the influence of design parameters on the rolling resistance of a tyre rolling on a specific road surface.

In this work a previously developed tyre/road interaction model is extended to account for different tread patterns and for losses due to small-scale tread deformation. Calculated contact forces and tyre vibrations for tyre/road interaction under steady-state rolling are used to predict rolling losses in the tyre. Rolling resistance is calculated for a series of different tyre/road combinations. Results are compared with rolling resistance measurements. The agreement between simulations and measurements is generally very good. It is found that both the tyre structure and small-scale tread deformations contribute to the rolling losses. The small-scale contribution depends mainly on the road roughness profile. The mean profile depth of the road surface is identified to correlate very well with the rolling resistance. Additional calculations are performed for non-traditional rubberised road surfaces, however, with mixed results. This possibly indicates the existence of additional loss mechanisms for these surfaces.

*Keywords:* tyre/road interaction, rolling resistance, parameter study, surface properties, tread pattern, numerical simulation

---

## 1. Introduction

In 2006 23 % of the CO<sub>2</sub> emissions in the European Union were due to the fuel consumption of the road transportation sector. For cars powered by classical combustion engines, only about 10 % to 40 % of the chemical energy stored in the fuel is available as mechanical energy from the engine. The other part is lost in the form of waste heat because of engine inefficiency [1]. The available energy is consumed by aerodynamic drag, rolling resistance and acceleration. Depending on driving conditions, hysteretic losses in the tyres, i.e. rolling resistance, eventually account for 5 % to 30 % of the fuel consumption of a typical passenger car [1]. These figures are even higher for trucks and other heavy vehicles, ranging from 15 % to 40 %. Accordingly, there is a

---

<sup>☆</sup> © 2015, Elsevier. Licensed under the Creative Commons Attribution-NonCommercial- NoDerivatives 4.0 International <http://creativecommons.org/licenses/by-nc-nd/4.0/>

\*Corresponding author. Tel. +46 31 772 8605

Email address: [carsten.hoever@chalmers.se](mailto:carsten.hoever@chalmers.se) (Carsten Hoever)

Preprint submitted to *Journal of Sound and Vibration*

1st June 2015

large potential to reduce a vehicle's overall fuel consumption by decreasing energy losses due to rolling resistance. A 10 % to 20 % reduction in rolling resistance is for example believed to reduce the fuel consumption within the EU by up to 2.5 % for passenger cars and 3.6 % for heavy vehicles [2]. Additionally, it has also been shown that the release of local pollutants such as CO and NO<sub>x</sub> can be reduced by lower rolling resistances [1].

Hybrid and electrically powered cars have a greatly improved power train efficiency when compared to vehicles with combustion engines. This implies that for this new type of vehicles the influence of the rolling resistance on the overall energy efficiency is even bigger. To conclude, a reduction of rolling resistance is essential for a more environmentally friendly road transportation sector.

Both tyre and road design can be utilised to reduce rolling resistance. In both cases a reliable model is needed which is able to quantify the influence of design parameters on the resulting rolling resistance. Obviously, it is desirable to be able to use the same model for road and tyre design purposes.

Numerous examples of calculations of rolling resistance are available in the literature (see [3] for an overview). Besides some approaches partly based on measured data [4, 5], most of them follow the same conceptual approach of using a steady-state rolling tyre model to calculate rolling resistance either as a drag force or based on energy dissipation.

A stationary tension band on an elastic foundation was used by Stutts and Soedel [6] to model the tyre; rolling resistance was then calculated from the deflection in the contact zone. In [7] hysteretic energy dissipation is determined from a model of an elastic ring supported by a viscoelastic foundation. Several other analytical methods for computing rolling resistance, including a flexible ring model, are compared in [8]. All these tyre models, however, are geometrically over-simplified, limiting their usefulness for tyre design purposes.

Finite element modelling (FEM) of the tyre is another very common approach, often combining mechanical and thermal models. Typically, the heat generation rate is calculated from a viscoelastic model of a free rolling tyre. Thermal simulations give the rolling resistance from the hysteresis. Models following this approach are e.g. [9–12]. In a more recent work this approach was used by Cho *et al.* [13] to investigate the influence of different tread patterns on rolling resistance. A slightly different technique was used by Ghosh *et al.* [14], who calculated the dissipated energy directly out of the strain energy density distribution in a steady-state rolling FE model. Another method which directly computes the energy loss during the mechanical FEM process was introduced as the *directional incremental hysteretic model* in [15]. Recently, Ali *et al.* [16] calculated the rolling resistance of a heavy truck tyre rolling on different non-smooth surfaces from reaction forces obtained by FE simulations. As the road surface profiles were artificially created no comparison to measurements could be made. The advantage of FEM approaches is that it is usually possible to use commercial software, thus reducing the implementation effort. The models are also rather geometrically detailed, allowing the extraction of information on the distribution of dissipation inside the tyre, thus aiding in the design process.

A general problem with all mentioned methods is the contact implementation. The used tyre/road interaction models are usually limited to the large scale deformations caused by static loading of a tyre rolling under steady-state conditions on a smooth road. Even in the few cases where non-smooth surfaces are considered the contact resolution is very coarse: in [16], for example, contact is calculated based on a tyre circumference divided into 60 segments. For the considered heavy truck tyre this corresponds to a contact patch size of 6 cm or more. Accordingly, the small scale variations of road roughness and the complex interrelation between tyre deformation and contact forces, which are both essential for the correct modelling of tyre vibrations, are

typically ignored in FE simulations. Recently, Boere *et al.* [17] proposed a two-step process to overcome this limitation. It superposes a dynamic local tread/road interaction on the large scale deformations obtained from FEM. Rolling resistance is calculated by means of input power into the system. Comparison of results to measurements showed that while rolling resistance was generally overestimated, correct tendencies for different road surfaces were obtained. A limitation of the implementation is that only 2D road roughness data, i.e. without lateral variation, is considered, and that there is no interaction between the tread/road and large-scale-deformation stages.

Another approach has been used by Fraggstedt [18]. He calculated the vibrations and rolling losses of a rolling tyre with a waveguide finite element model (WFEM). Frequency and wave order distributions were shown together with individual element contributions to the overall dissipation. However, the deviations between simulated and measured rolling resistances were slightly higher than for some of the other mentioned methods. Furthermore, only a few different road surfaces were considered and a detailed analysis of the results was missing.

An extension of the approaches suggested by Fraggstedt and Boere *et al.* is used in the work presented in this paper. Rolling resistance can either be defined as the drag force  $F_R$  acting in opposite direction to the rolling of the tyre, or, as is done in ISO 18164:2005 [19], as the dissipated energy  $E_{\text{diss}}$  over the distance of rolling  $L$ . Normalising with the total averaged radial contact force  $F_c$ , the rolling resistance coefficient  $C_r$  for steady-state rolling at speed  $V$  is obtained as

$$C_r = \frac{F_R}{F_c} = \frac{E_{\text{diss}}}{F_c L} = \frac{P_{\text{diss}}}{F_c V}, \quad (1)$$

where  $P_{\text{diss}}$  is the dissipated power. Due to conservation of energy, and under the assumption that frictional losses can be ignored for steady-state rolling, the power input into the tyre through the contact,  $P_{\text{in}}$ , is identical to the lost power, i.e.  $P_{\text{diss}}$ . For a discrete description of the lateral contact position the time-average input power for steady-state rolling is given as

$$P_{\text{in}} = \frac{1}{T} \sum_i \int_0^{2\pi} \int_0^T F_i(t, \theta) \frac{\partial v_i(t, \theta)}{\partial t} dt d\theta. \quad (2)$$

Herein,  $F_i$  and  $\partial v_i / \partial t$  denote the radial contact force and radial tyre velocity for the lateral contact track  $i$ ,  $T$  is the evaluation time, and  $\theta$  the circumferential angle.

This means that the rolling resistance can be expressed in terms of the time-varying contact forces and tyre deformations as given by a dynamic tyre/road interaction model typically used for tyre/road noise calculations. The use of such a model ensures detailed modelling of the tyre, the road, and their interaction, as this is a prerequisite for successful tyre/road noise simulations. Moreover, the distributions of rolling losses for different frequencies or circumferential orders of tyre vibrations can be analysed [18, 20].

The starting point of the work presented in this paper is the tyre/road interaction model which originally had been developed by one of the authors [21]. During the last decades the model has been modified and extended [22–24]. It is based on a modular approach which allows to combine tyre, contact, radiation and/or rolling resistance models of any necessary complexity for the problem under investigation. The two core modules used for this work are a viscoelastic WFE tyre model and a non-linear time-domain based tyre/road contact model. With these tools the contact forces and tyre vibrations for tyre/road interaction under steady-state rolling can be calculated. Based on these properties rolling losses can be calculated from (2). The existing

contact formulation is extended to include non-linear damping. With this, rolling losses due to local deformation of the tread by road texture asperities can be determined. The tyre and contact models are also adjusted to account for the influence of tread patterns. From the AOT project [25] road surface profiles for a variety of different test sections at the Kloosterzande test site in the Netherlands are available to the authors. In [26] results for rolling resistance measurements for two different tyres on exactly the same test fields are reported. In the present study rolling resistance simulations are conducted with the aim of reproducing the results obtained in [26]. The results further allow to investigate the influence of the surface roughness on the rolling resistance. A few non-traditional poroelastic or rubberised road surfaces are examined as well.

Although this paper mainly focuses on the influence of road texture and tyre tread pattern on rolling resistance, the applied model is also applicable for investigating improved tyre design solutions. This is shown by calculating rolling resistance by means of the internal dissipation inside the tyre for some of the road surfaces.

The paper is organised as follows. In Section 2 a brief introduction into the models for the tyre vibrations and the tyre/road interaction is given. It is explained how the rolling resistance is calculated and how the influence of the tread pattern can be included in the simulations in an efficient way. Section 3 gives an overview of the different considered road surfaces and their main properties. Simulated and measured rolling resistances for different tyres and road surfaces are compared in Section 4. In Section 5 the method is tested for the rubberised surfaces. Conclusions are finally given in Section 6.

## 2. Calculating rolling resistance

### 2.1. The waveguide finite element tyre model

Traditionally, analytical models based on plates (e.g. [22, 27]) or cylindrical rings (e.g. [21, 28, 29]), or numerical FE models (e.g. [17, 30]) have been used to model the vibrational behaviour of tyres. In recent years several approaches combining parts of conventional FE modelling with analytical methods have been presented, for example by Nilsson [31] or Waki *et al.* [32]. Nilsson’s approach, the waveguide finite element method, was later used by Sabiniarz and Kropp [33] to investigate the vibrational behaviour of tyres. The model is detailed, yet computationally very efficient and has been validated against input and transfer mobility measurements. It has also successfully been used for the calculating of tyre/road noise [24], and is the basis for the tyre modelling in the present study. In the following a brief overview of the model is given, more details can be found in [24, 33].

A waveguide is a system with constant geometrical and material properties along one (typically “long”) dimension. In this dimension, the motion can be described by a set of propagating waves fulfilling the boundary conditions imposed by the waveguide characteristics. For a tyre motion along the circumferential dimension can be described by waves fulfilling a periodicity condition  $u(\theta) = u(\theta \pm 2\pi)$ , where  $u$  is the tyre displacement and  $\theta$  the circumferential angle. The tyre cross-section is modelled similar to a conventional two-dimensional FEM approach, see Fig. 1a. For a cylindrical coordinate system as shown in Fig. 1b the components of the displacement vector  $\mathbf{u} = [u_r \ u_x \ u_\theta]^T$  (with  $(\bullet)^T$  denoting vector transpose) at a point  $(r, x, \theta)$  are accordingly given by

$$u_i(r, x, \theta, t) = \mathbf{N}(r, x) \mathbf{v}_i(\theta, t), \quad i = r, x, \theta. \quad (3)$$

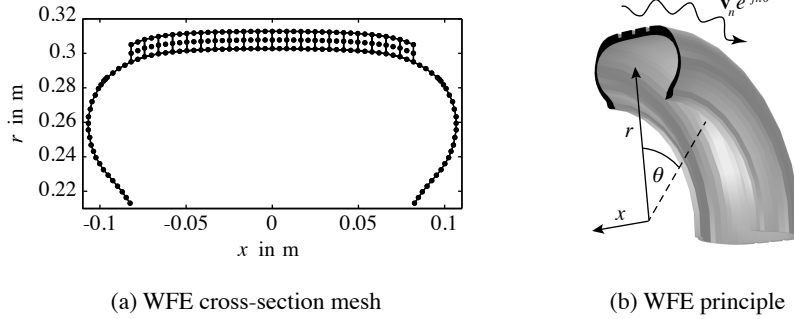


Figure 1: (a) WFE mesh of the 205/55 R16 tyre cross section. Nodes marked by  $\bullet$ . (b) The tyre as a curved waveguide: for the cross-section (marked in black) in the  $(x, r)$ -plane an FE approximation is used, while in circumferential direction  $\theta$  wave propagation is assumed. Waves traveling in negative  $\theta$  direction have to be considered as well, but are not shown here.

Herein,  $\mathbf{N}$  is a vector of cross-sectional FE shape functions while  $\mathbf{v}_i$  represents the corresponding nodal degrees of freedom vector. Thus, only the displacements' dependence on the cross-sectional coordinates is approximated using FE modelling. The nodal displacements are functions of the angular coordinate  $\theta$  and depend on the assumed wave propagation along this dimension.

The engineering strain vector  $\varepsilon$  is given in the bi-linear form

$$\varepsilon(r, x, \theta) = \mathbf{E}_0(r, x)\mathbf{v}(\theta) + \mathbf{E}_1(r, x)\frac{\partial\mathbf{v}(\theta)}{\partial\theta}, \quad (4)$$

where  $\mathbf{v}$  is the vector of all nodal displacements, and  $\mathbf{E}_0$  and  $\mathbf{E}_1$  are matrices depending on the element-specific strain-displacements relations and shape functions and their derivatives. Using Hamilton's approach and assuming viscoelastic material properties, harmonic motion of type  $e^{j\omega t}$  (where  $\omega$  is the angular frequency and  $j = \sqrt{-1}$ ), and the absence of volume forces and external traction, a set of coupled ordinary differential equations [34] is obtained:

$$\left[ -\mathbf{A}_{11}\frac{\partial^2}{\partial\theta^2} + (\mathbf{A}_{01} - \mathbf{A}_{10})\frac{\partial}{\partial\theta} + \mathbf{A}_{00} - \omega^2\mathbf{M} \right] \mathbf{v}(\theta, \omega) = \mathbf{f}(\theta, \omega). \quad (5)$$

The generalised stiffness matrices  $\mathbf{A}_{kl}$  and the mass matrix  $\mathbf{M}$  are derived from the tyre's potential and kinetic energies, and can be complex to account for damping.  $\mathbf{f}$  is the generalised force vector describing the external load. The solutions for the homogeneous case  $\mathbf{f} = 0$  are given as

$$\mathbf{v}(\theta, \omega) = \mathbf{v}_n(\omega)e^{-jn\theta}. \quad (6)$$

These functions are waves of cross-sectional mode shape  $\mathbf{v}_n$  propagating along the circumferential direction with polar wave order  $n$ , see Fig. 1b. Inserting (6) into (5) results in an eigenvalue problem which can be solved to get the eigenfrequency and -vector for a specific value of  $n$ .

Likewise, the inhomogeneous form of (5) for a particular wave order  $n$  is obtained as

$$\left[ \mathbf{A}_{00} - jn\mathbf{A}_{01} + jn\mathbf{A}_{10} + n^2\mathbf{A}_{11} - \omega^2\mathbf{M} \right] \mathbf{v}_n(\omega) = \mathbf{F}_n(\omega). \quad (7)$$

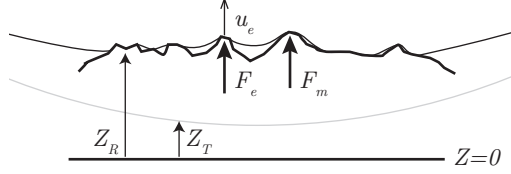


Figure 2: Contact geometry between tyre and road. The reference surface is located at  $Z = 0$ , the undeformed tyre contour (grey) is given by  $Z_T$  and the road roughness profile by  $Z_R$ .  $F_e$  and  $F_m$  are the contact forces acting at points  $e$  and  $m$ , and  $u_e$  is the dynamic response of the structure in point  $e$ .

Herein,  $\mathbf{F}_n(\omega)$  results from the expansion of  $\mathbf{f}(\theta, \omega)$  with respect to the circumferential wave order  $n$ . For a tyre circumference which is discretised into  $C$  equidistant intervals of length  $\Delta$  it is given as [24]

$$\mathbf{F}_n(\omega) = \sum_{c=1}^C \mathbf{F}_{\text{lat}}(\theta_c, \omega) \frac{\sin(n\Delta/2)}{n\pi\Delta} e^{jn\theta_c}, \quad (8)$$

where  $\mathbf{F}_{\text{lat}}(\theta_c, \omega)$  is the force variation over the tyre cross-section in the circumferential segment  $[\theta_c - \Delta/2, \theta_c + \Delta/2]$ .

Eq. (7) can for example be solved using a modal summation procedure as described in [24]. While numerically efficient, this procedure can only be applied for proportional damping, i.e. when the same loss factor applies to entries of  $\mathbf{A}_{kl}$  in (7). For rolling resistance modelling it is desirable to assign different loss factors to for example the highly-damped tread rubber and the less damped carcass. For this non-proportional damping the response for a particular wave order  $n$  can be calculated by direct matrix inversion of (7), i.e.

$$\mathbf{v}_n(\omega) = [\mathbf{A}_{00} - jn\mathbf{A}_{01} + jn\mathbf{A}_{10} + n^2\mathbf{A}_{11} - \omega^2\mathbf{M}]^{-1} \mathbf{F}_n(\omega). \quad (9)$$

The total response is then given as summation of (9) over all circumferential wave orders  $-N \leq n \leq N$  (where negative  $n$  denote waves travelling in negative  $\theta$ -direction).

## 2.2. Tyre/road interaction

For the analysis a tyre/road interaction model is required which ensures that the time-changing contact geometry and force distribution are captured realistically. The contact can be considered as having a mixed boundary condition where the displacement of the tyre in the contact area is prescribed by the contour of the tyre, the tyre vibrations, and the road surface texture. In order to fulfil the contact geometry, contact forces are needed which ensure the required deformations of the tyre. The model used here is based on the convolution approach originally developed for tyres by one of the authors [21], and its subsequent enhancements by several authors [35–37]. Only contact deformations and forces in normal direction are considered.

The time-dependent position of a point  $e$  on the tyre surface can be written as

$$Z_e(t) = Z_{T,e}(t) + u_e(t), \quad (10)$$

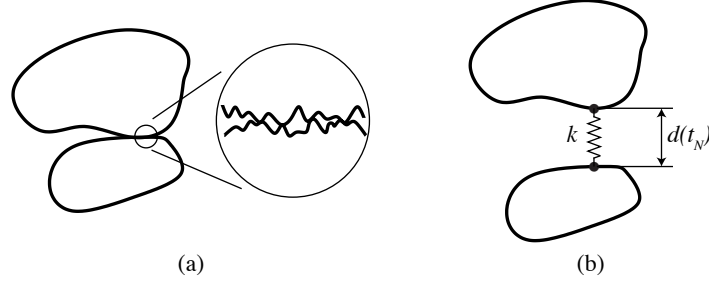


Figure 3: (a) Due to the small-scale surface roughness the real area of contact is smaller than the apparent. (b) contact springs are introduced to account for this effect.

where  $Z_{T,e}(t)$  is the position of the tyre contour (which could include a tread pattern) as shown in Fig. 2. The tyre vibration  $u_e(t)$  is caused by present and past forces. It is given by the convolution

$$u_e(t) = \sum_m \int_{-\infty}^{\infty} F_m(\tau) g_{m,e}(t - \tau) d\tau. \quad (11)$$

where  $g_{m,e}$  is the displacement Green's function for a point  $e$  due to a contact force  $F_m$  at point  $m$ . It is obtained by an inverse Fourier transform of input and transfer receptances which are calculated from the WFE tyre model. Assuming causality and that the system is at rest for times  $t < 0$ , a time discretised version of (11) for  $t_n = n\Delta t$  (with  $n = 0, 1, \dots, N$ ) is obtained as

$$u_e(t_N) = \sum_m \sum_{n=0}^N F_m(t_n) g_{m,e}(t_N - t_n) \Delta t \quad (12a)$$

$$= \sum_m F_m(t_N) g_{m,e}(0) \Delta t + \sum_m \sum_{n=0}^{N-1} F_m(t_n) g_{m,e}(t_N - t_n) \Delta t \quad (12b)$$

$$= \sum_m F_m(t_N) g_{m,e}(0) \Delta t + u_e^{\text{old}}(t_N). \quad (12c)$$

The contact forces in the second term of (12b) are known from the previous time steps. This means that in each time step the term  $u_e^{\text{old}}(t_N)$  can be calculated separately before the contact problem is solved. As a matrix expression for all possible contact points  $e = 1 \dots M$ , (12c) reads

$$\mathbf{u}(t_N) = \mathbf{G}_0 \mathbf{F}(t_N) + \mathbf{u}^{\text{old}}(t_N). \quad (13)$$

Here,  $\mathbf{G}_0$  is a  $M \times M$  matrix containing the values of the Green's functions for  $t = 0$ , and the term  $\Delta t$ . The distance between tyre contour and road is given by

$$\mathbf{d}(t_N) = \mathbf{Z}_R(t_N) - \mathbf{Z}_T(t_N) - \mathbf{u}(t_N), \quad (14)$$

where  $\mathbf{Z}_T$  contains all  $Z_{T,e}$ , and  $\mathbf{Z}_R$  is the three-dimensional road surface roughness. A positive entry  $d_e$  in (14) indicates that the road penetrates into the tyre at the particular contact point  $e$ .

Equations (10) to (14) formulate a continuum mechanics based description of the tyre/road contact for length scales down to the used tyre discretisation. However, small-scale roughness

phenomena can have a considerable effect on the contact behaviour. The difference between the apparent and the real area of contact (which is much smaller than the apparent one) affects the contact stiffness, see Fig. 3(a). One solution to account for this is to use a sufficiently fine resolution of the contact zone. Yet, with respect to the necessary numerical effort, this is often not reasonable. As is shown in Fig. 3(b), contact springs can instead be introduced between the possible points of contact on the tyre and the road to account for the difference in stiffness [36].

A similar argument can be made for rolling losses induced by the small-scale road roughness. The interaction between the road asperities and the highly damped tread rubber is not adequately represented by a contact resolution which is within numerically reasonable limits. The losses due to the small-scale tread deformations can instead be included as an additional damping term in the expression for the contact force at a point  $e$ :

$$F_e(t_N) = \left[ k_e d_e(t_N) + c_e d_e(t_N) \frac{\partial}{\partial t_N} d_e(t_N) \right] \cdot \mathcal{H}\{d_e(t_N)\}. \quad (15)$$

$\mathcal{H}$  is the Heaviside function, and  $k_e$  and  $c_e$  denote the contact spring stiffness and damping coefficient. In (15) a special non-linear damping expression is used. Compared to viscous damping it has the advantage of resulting in a physically more reasonable hysteresis loop [38]. In particular does it not lead to a discontinuous contact force at initial contact and separation. Damping also depends on the indentation which is physically reasonable as the contact area increases with deformation. Because of these properties and its relative simplicity, it is a widely used formulation in impact modelling (for an overview see the review article [39]). The damping coefficient  $c$  is usually determined as a global parameter from the coefficient of restitution [38]. As this approach is not readily applicable to the rolling tyre/road interaction, and as there is no reason to not allow individual  $c_e$  for each contact point  $e$ , another approach is chosen here, see Sections 2.4 and 2.5.

In contrast to the model described in [36], only linear contact springs are used here. This is motivated by the fact that the resolution of the available road roughness data is not sufficient<sup>1</sup> for a proper estimation of the non-linear stiffnesses as outlined in [36]. This implies that the difference between the real and apparent area of contact is included in the contact model, while the change in contact area during contact is not.

Equations (13) to (15) formulate a non-linear contact problem. This is solved iteratively for every time-step using a Newton-Raphson algorithm to obtain the contact forces. After Fourier transformation to the frequency domain the forces are used as excitation for the WFE tyre model. The result is the vibrational field of a tyre rolling on a road which can be used as input into the rolling loss model.

### 2.3. Rolling losses

In the time-space-domain rolling losses can directly be calculated from the input power Eq. (2). In [18] it is shown that the same expression in the frequency and circumferential wave order domain is given as

$$P_{\text{in}} = 2\pi \sum_{n=-N}^N \sum_{m=0}^M j\omega_m \left( \mathbf{F}_{-n}^H(\omega_m) \cdot \mathbf{v}_{-n}(\omega_m) - \mathbf{F}_n^T(\omega_m) \cdot \mathbf{v}_n^*(\omega_m) \right), \quad (16)$$

---

<sup>1</sup>The available resolution is 0.2 mm, in [36] 38  $\mu\text{m}$  was used.

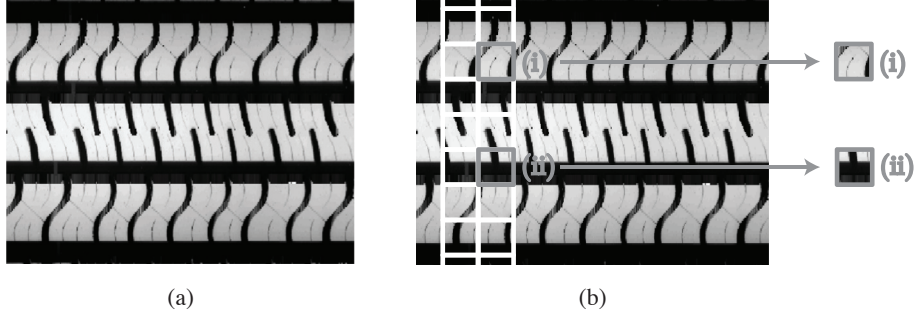


Figure 4: (a) Example of a tread pattern. (b) Scheme for scaling the contact stiffnesses by the amount of rubber in the respective contact patch. There is more rubber in patch (i) than in patch (ii). Accordingly the local contact stiffness in (i) will be nearly unchanged while it will be very little in (ii), i.e.  $k_i \gg k_{ii}$ .

with  $(\bullet)^H = (\bullet)^{T*}$ , and  $(\bullet)^*$  being the complex conjugate. The nodal displacements and forces,  $\mathbf{v}_{\pm n}$  and  $\mathbf{F}_{\pm n}$ , are given by equations (8) and (9). Eq. (16) conveniently allows the identification of the contribution of individual wave orders or frequencies to the rolling losses. Moreover, as the stiffness and mass matrices in (9) are assembled from element-specific components, (16) can be decomposed into a sum of element contributions. This allows to identify the spatial distribution of the internally dissipated power over the tyre cross section.

The rolling losses due to small-scale tread indentation are given by a discrete version of (2)

$$P_{\text{tread}} = \frac{1}{T} \sum_{i=0}^l \sum_e c_e d_{i,e} \left( \frac{\partial d_{i,e}}{\partial t} \right)^2 \Delta t, \quad (17)$$

where  $T = l\Delta t$ .

The rolling resistance coefficient  $C_r$  is finally calculated based on the sum of the large-scale tyre and small-scale tread losses, i.e.  $P_{\text{diss}} = P_{\text{in}} + P_{\text{tread}}$  in (1).

#### 2.4. Influence of the tread pattern

The influence of the tread pattern is twofold. Geometrically it influences which areas of the tyre are in contact with the ground. This also results in a variation of the local contact stiffness. Additionally, the tread pattern influences the dynamic tyre response. Studies have shown that the eigenfrequencies of typical tread blocks of passenger car tyres are very high in frequency [40]. This indicates that details of the block dynamics might not be particularly important for the rolling resistance simulations as it has been shown that rolling losses are mainly a low frequency phenomenon [18, 20]. While an explicit modelling of tread blocks is not necessary, there is an influence of the presence of voids in the rubber on the tread's mass and stiffness. This is a global effect which can be handled by mass and stiffness adjustments of the solid elements forming the tread layer. In conclusion, the tread pattern is modelled by a spatially varying stiffness in the tyre/road interaction, and by mass and stiffness adjustments of the tread layer in the tyre model.

A typical tyre profile is shown in Fig. 4(a). It is possible to include such a tread pattern in the tyre/road contact simulations via the tyre profile  $\mathbf{Z}_T$  in (14). However, the needed spatial discretisation is so fine that computational burden would be extreme; not only for the contact modelling but also for the tyre response calculations. To keep the numerical effort reasonable, a different

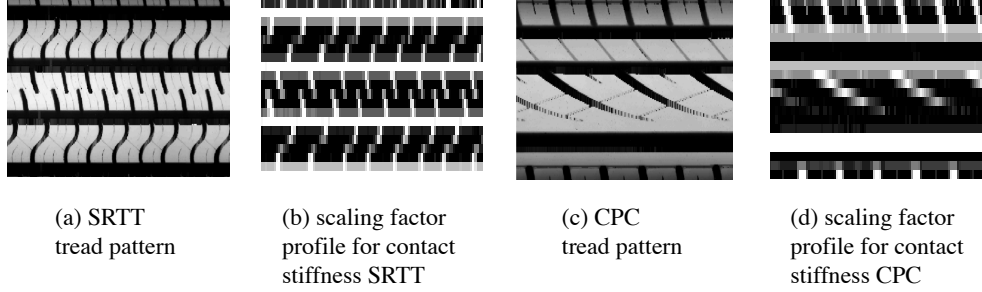


Figure 5: Sections of the tread pattern (a/c) and the corresponding contact stiffness scaling factors  $\Phi_{e,r}$  (b/d) of the two tyres. All sections have approximately the same dimensions of  $15 \text{ cm} \times 15 \text{ cm}$ . Solid white represents a scaling factor of zero and solid black a factor of one in (b/d).

approach is chosen. Fig. 4(b) shows the main idea in a schematic way. Based on the lateral and circumferential contact resolution, the whole tread over the tyre width and circumference is divided into small areas, each representing one individual contact point  $e$  in (15). For each of these areas the surface fraction of rubber can be determined in advance as

$$\Phi_{e,r} = \frac{A_{e,r}}{A_{e,r} + A_{e,v}}, \quad (18)$$

where  $A_{e,r}$  and  $A_{e,v}$  denote the rubber and void areas in the contact patch  $e$ .  $\Phi_{e,r}$  is then used to scale the local contact stiffness, i.e.  $k_e$  is replaced by  $k'_e = k_e \Phi_{e,r}$  in (15). A similar approach has been successfully used in the SPERoN model [41]. The damping coefficient  $c_e$  is scaled in the same way.

The lateral size of a contact patch in the tyre/road interaction calculations is equivalent to the width of a solid element in the tyre cross-section mesh in Fig. 1(a). By averaging  $\Phi_{e,r}$  over the circumference a scaling factor for the stiffness and mass of each solid element is obtained. These scaling factors are applied to the corresponding elements when assembling  $\mathbf{A}_{kl}$  and  $\mathbf{M}$  in (5).

### 2.5. Tyre input data

In [26] rolling resistance measurements were conducted for two different 225/60 R16 tyres: a Uniroyal Tigerpaw standard reference test tyre (SRTT) and a Continental CPC2 LI98 (CPC). The tread patterns of these two tyres and the corresponding local stiffness scaling factor profiles are shown in Fig. 5. As no material input data was available for these two tyres, an existing tyre model based on a slick Continental 205/55 R16 tyre was used as basis for both tyres in the present study. This tyre has successfully been validated against measured input and transfer mobilities, see Fig. 6,<sup>2</sup> and rolling noise measurements [24]. Using this tyre is deemed a viable solution as the study focuses on qualitative effects of tread pattern and road surface. In addition to the SRTT and the CPC tyres, simulations are also performed for a slick tyre without any profile, even though no measurement data is available for this tyre. This is done to further evaluate the influence of the tread pattern on the rolling resistance.

<sup>2</sup>In [33] more examples for measured and simulated mobilities can be found, albeit using a different damping model in the simulations.

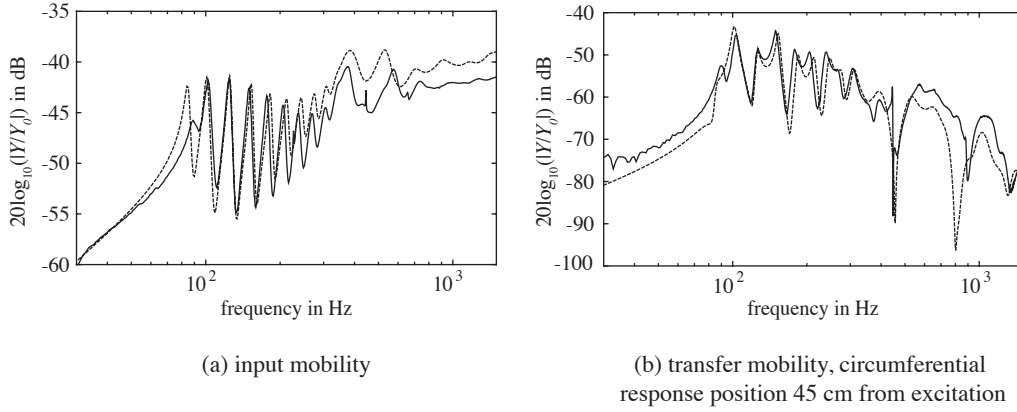


Figure 6: Comparison of radial input and transfer mobilities  $Y$  from measurements (—) and simulations (---). Excitation and response at tread centre line. Additional first resonance in simulations in (a) due to differences in boundary conditions between measurements and simulations.  $Y_0 = 1 \text{ N/(ms)}$ .

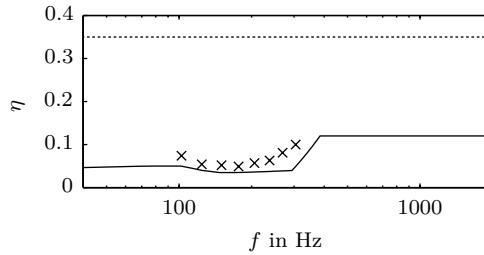


Figure 7: Loss factors for the shell (—) and solid (···) elements. Results from half-power bandwidth measurements marked by  $\times$ .

The cross-sectional tyre mesh is shown in Fig. 1(a). It consists of 46 deep shell elements for the sidewalls and belt, and 20 quadrilateral 9-node Lagrangian solid elements for the tread. Detailed descriptions of both element types are given in [34]. The rim and the air cavity are not explicitly modelled, but their effect is included by blocking the tyre motion at the bead and including the pre-tension due to inflation. The resolution around the tyre circumference is 1024 steps. Each of the 20 solid elements also acts as a lateral contact track in the contact simulations. This is a sufficiently high number for rolling tyre simulations [42]. The tread patterns are not explicitly modelled; they are included in the tyre and contact simulations as outlined in Section 2.4.

Damping is implemented by complex stiffness matrices  $\mathbf{A}_{kl}$  in (5). Contrary to the tyre/road noise calculations performed for the same tyre in [24], the use of proportional damping is no longer appropriate. Instead different loss factors  $\eta$  are assigned to the shell and the solid elements. As no loss factor data was provided by the manufacturer, values for  $\eta$  are determined manually. Based on half-power bandwidth estimations for resonances in a measured input mobility, the loss factor can be estimated in the 100 Hz to 300 Hz region. Values outside this region and the distribution of losses between solid and shell elements is determined by matching simulated mobilities to measured ones, see Fig. 6. This results in a frequency-dependent loss factor for

Table 1: Considered road surfaces.

road type	abbreviation	aggregate size (layer thickness)
artificial smooth surface	smooth	-
ISO 10844 reference surface [43]	ISO	-
dense asphalt concrete	DAC	0/16
thin-layered asphalt	TLA	2/4, 2/6, 4/8
stone mastic asphalt	SMA	0/6, 0/8, 0/11, 0/16
porous asphalt concrete	PAC	2/4, 2/6, 4/8, 0/11, 8/11 (45mm), 8/11 (200mm), 0/16
surface dressing	SD	5/8, 11/16

the shell elements as shown in Fig. 7. For the solid elements representing the highly damped rubber a constant loss factor of 0.35 is used. The remaining material data was provided by the manufacturer, details about it can be found in [33].

For the tyre/road interaction modelling a contact spring stiffness of  $k_e = 1.25 \cdot 10^4 \text{ N}\cdot\text{m}^{-1}$  is used as starting value before the adjustment for the tread pattern. This stiffness results in a contact patch which is of the right size for the considered tyre dimensions, inflation pressure, and axle load. Since the damping coefficient  $c_e$  is very difficult to determine experimentally for a tyre/road contact, an engineering approach was used to estimate it. Looking at the rolling losses, a  $c_e$  was chosen which fulfils two conditions. For an artificial, completely smooth surface without any small-scale roughness,  $P_{\text{tread}}$  is required to be zero. Simultaneously, the chosen  $c_e$  should lead to rolling resistances which accurately predict the relative differences between the roughest surfaces, i.e. those for which the influence of the small-scale tread deformations are strongest. These conditions result in a damping coefficient of  $c = 3.25 \text{ Ns}\cdot\text{m}^{-2}$  before tread pattern adjustment.

A driving speed of 80 km/h, an axle load of 4100 N, and an inflation pressure of 200 kPa are assumed. Rolling is calculated for five full tyre revolutions of which the last one is used to calculate  $P_{\text{in}}$  and  $P_{\text{tread}}$  from Equations (16) and (17).

### 3. Road properties

Simulations are performed for the 19 road surfaces given in Tab. 1. All surfaces apart from the smooth one are test fields at a dedicated test site in Kloosterzande, the Netherlands [25]. For each surface texture scans were performed at six different positions in the corresponding test field. The determination of road properties and the rolling resistance calculations are performed individually for all of the available profile scans for each surface. In the following the average of these results is typically presented. Comments on variations between scans of the same surface are made if necessary.

Each scan consists of 20 parallel tracks of length 2.95 m and a lateral spacing of 0.01 m. The resolution in rolling direction is 0.2 mm for all road surfaces. For the contact simulations, all surface scans are resampled to match the resolution of the tyre model, giving a circumferential contact resolution of 1.9 mm.

A single-value characterisation of the road surface profiles is possible by means of the root mean square deviation of the profile  $RMS$ , and the mean profile depth  $MPD$ , both of which are

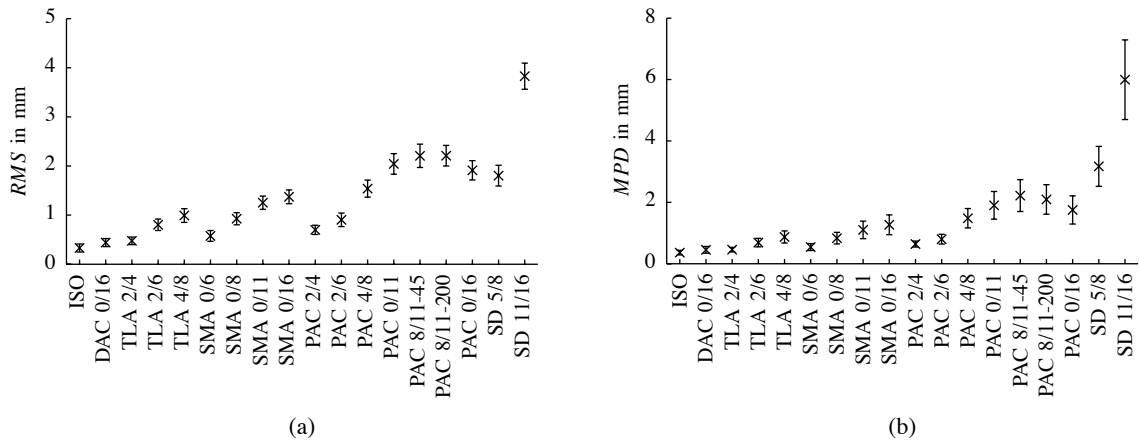


Figure 8: Average of (a) the road mean square deviations (*RMS*), and (b) the mean profile depth (*MPD*) for all road surfaces. Average based on all measurement positions and all tracks. Errorbars indicate standard deviation.

defined in ISO 13473-2 [44]. Results are shown in Fig. 8. While both parameters seem to correlate approximately with the maximum aggregate size of the road surface, there is considerable difference in how the SD 5/8 surface ranks with respect to the other surfaces. While it has the second largest *MPD* value, the *RMS* value is only the sixth highest; most of the PAC surfaces have a higher *RMS*. Additionally, the *MPD* has a considerably higher standard deviation for the rougher surfaces.

A further characterisation of the road surfaces is possible by the profile amplitude distributions shown in Fig. 9. Rougher surfaces, i.e. those with higher *MPD* or *RMS*, have flatter, broader amplitude distributions. The peak width seems to better correlate to the *MPD* than the *RMS*, cf. the width of the peak for the SD 5/8 in relation to the width of the PAC distributions. Some of the TLA, SMA, and PAC surfaces are also characterised by skewed distributions with maxima in the positive texture amplitude range.

In Fig. 10 the average road surface spectra  $L_{Tx}$  (calculated according to ISO 13473-4 [45]) are given. Above some 8 mm the order of the surfaces is similar to the one obtained for the *RMS*. The level differences between the spectra reach up to 25 dB for wave lengths larger than 16 mm. For smaller wave lengths the difference is up to 10 dB, with most surfaces being within 6 dB of each other. This emphasises the importance of an adequate representation of the small-scale tyre/road interaction to properly capture the texture differences between the surfaces at smaller wave lengths.

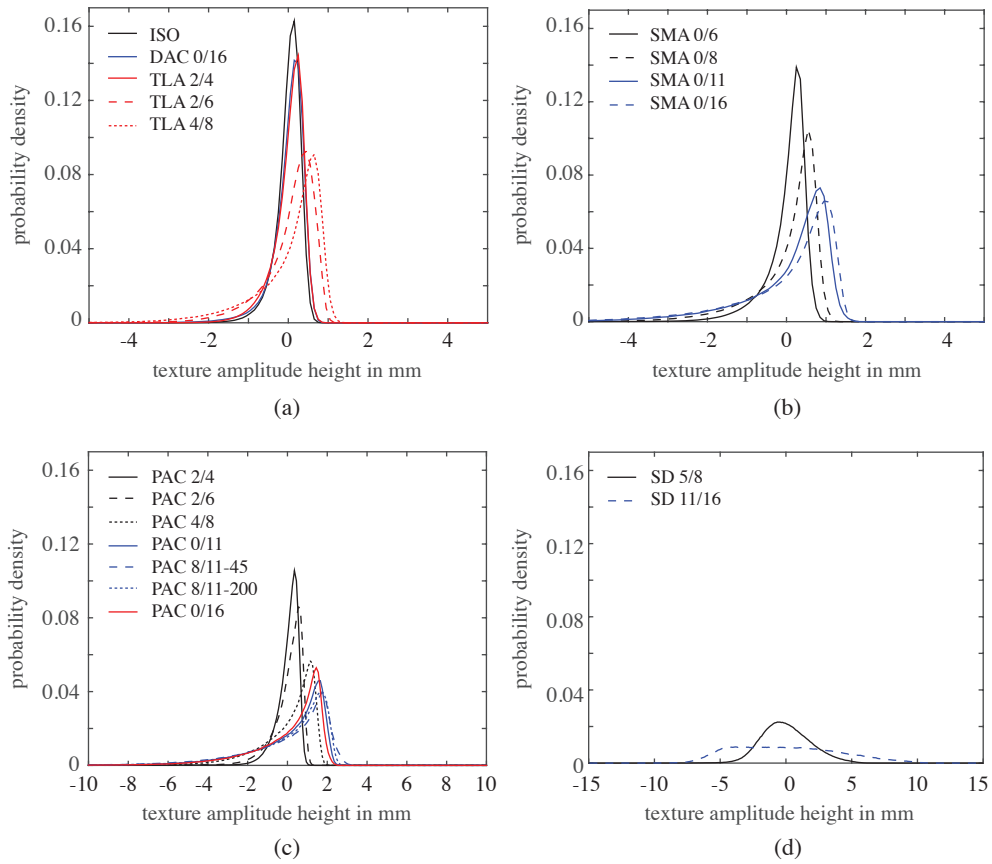


Figure 9: Profile amplitude distributions for the different surfaces. Note the differences in  $x$ -axis scaling.

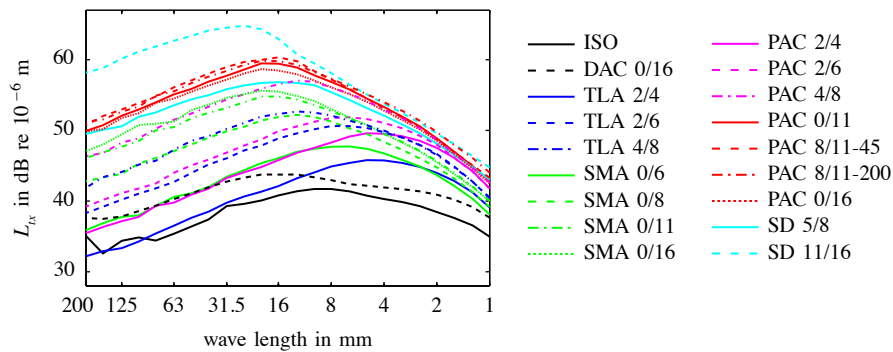


Figure 10: Average road surface spectra in third-octave bands. Average based on all measurement positions and all tracks. Spectra based on original surface scans before resampling to tyre resolution.

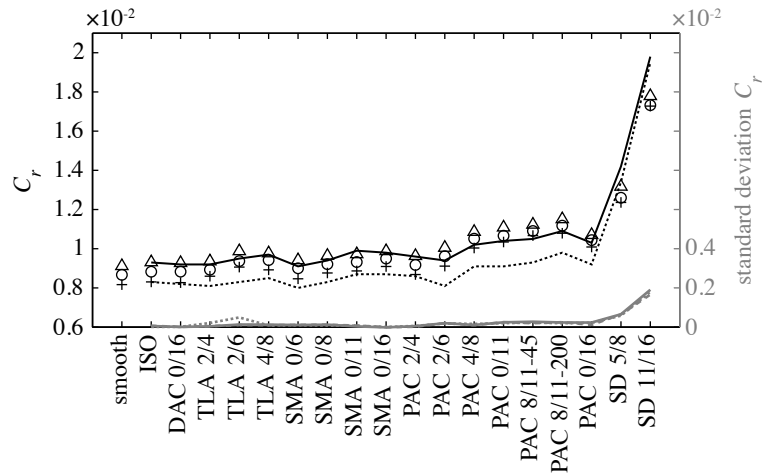


Figure 11: Left y-axis (black): rolling resistance for CPC measured (—) and simulated ( $\circ$ ), SRTT measured ( $\cdots$ ) and simulated ( $+$ ), and the simulated slick tyre ( $\Delta$ ). No measured data available for the slick tyre. Right y-axis (grey): standard deviation for CPC (—), SRTT ( $\cdots$ ), and the slick tyre ( $\rightarrow$ ). Note: identical step size on both y-axes.

#### 4. Rolling resistance for conventional road surfaces

Rolling resistance was measured at the same test site where also the road surface profiles were scanned. A trailer designed by the Technical University of Gdansk was used to directly measure the rolling resistance coefficient  $C_r$ . The measurements were conducted at a speed of 80 km/h and axle load of 4100 N [26].

Calculated and measured rolling resistances for the different road surfaces and tyres are shown in Fig. 11. For the CPC tyre a generally good agreement with the measurements is achieved. Absolute values and the relative ranking of the road surfaces are captured well with a slight underestimation of the measured values for most of the surfaces. Only the  $C_r$  values for the PAC surfaces, apart from the one with aggregate size 2/4, are overestimated by roughly 10%. The SD 11/16 in contrast, is underestimated by about the same margin. The measurements for the SRTT show a very similar behaviour to the CPC results but are around 5% lower for most of the surfaces. This is slightly less than in the measurements where the difference between CPC and SRTT is about 10%. This is possibly related to the fact that an identical tyre structure with only minor adjustments for the tread pattern is used to model both tyres. In reality there are differences in the tyre construction between the SRTT and the CPC, and this affects the rolling resistance as well.

No measured data is available for the slick tyre. Yet, the different road surfaces have a similar influence on the rolling resistance as for the two other tyres. However, the rolling resistance is always higher than for the two tyres with profiles. This agrees with the measurement results reported for other tyres in [46], and can be explained by the additional rubber material in the tread of a slick tyre [47]. For all tyres the lowest rolling resistance is obtained for the smooth surface.

Generally, the biggest difference between simulated and measured values is obtained for the SD 11/16 surface with an underestimation of the  $C_r$  by about  $0.2 \cdot 10^{-2}$ . For the SD 11/16

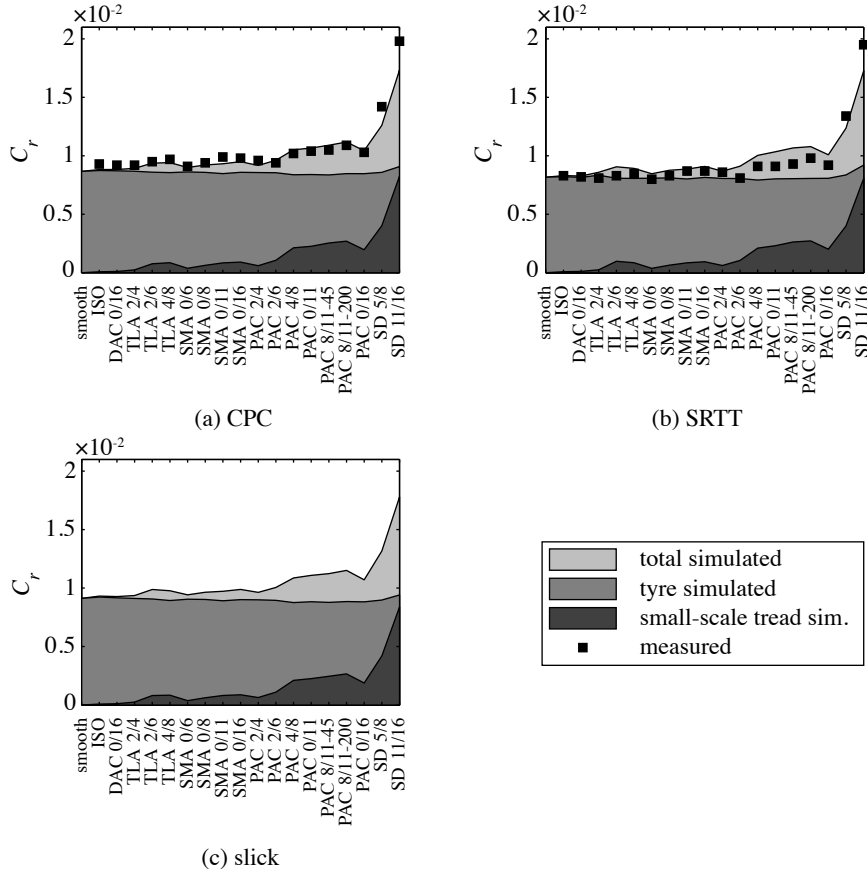


Figure 12: Contribution of tyre structure and small-scale tread deformation to the simulated rolling resistance of (a) the CPC, (b) the SRTT, and (c) the slick tyre (no measurement data available).

the standard deviation of  $C_r$  is the highest of all surfaces and of about the same order as the difference between simulations and measurements. It is not completely clear from [26] how the six different scans for each road surface and the driving track for the  $C_r$  measurements align, and how the averaging for the latter is done. Accordingly, the higher deviation between simulations and measurements might be explained by variations of the SD 11/16 surface over the complete test field. Another aspect which has to be considered is that an identical contact stiffness  $k_e$  is used for all road surfaces during the simulations. For most of the surfaces this is a valid simplification as their *RMS* or *MPD* are within the same limited range of values. This is not the case for the SD 11/16 surface and better match to measurements might be achieved by an appropriately adjusted contact stiffness.

Fig. 12 shows the distribution of the simulated rolling losses between large-scale tyre structure losses and small-scale tread losses. The contribution of the tyre structure to the rolling resistance,  $C_{r,tyre}$ , is nearly identical for all road surfaces; the range is in the order of  $0.08 \cdot 10^{-2}$  for all tyres. The absolute values originating from the tyre structure are slightly higher for the slick tyre, for which the average  $C_{r,tyre}$  is  $0.89 \cdot 10^{-2}$ , compared to  $0.85 \cdot 10^{-2}$  and  $0.86 \cdot 10^{-2}$  for

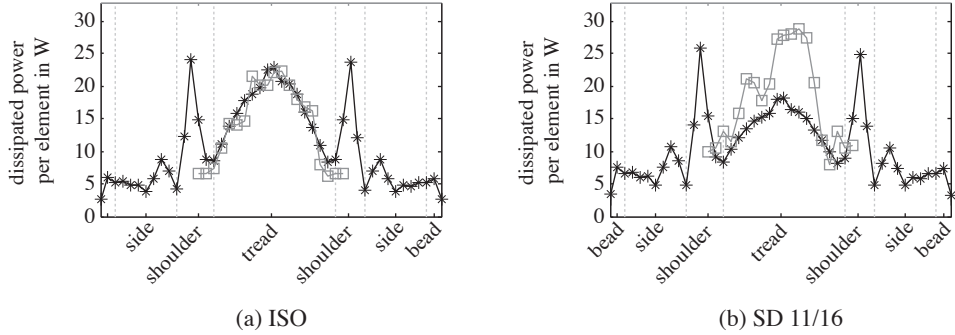


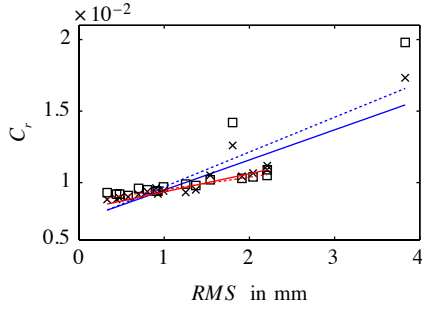
Figure 13: Distribution of dissipation over the CPC tyre cross-section. Each (\*) marks one shell element, each (□) one solid element. (· · ·) marks the different tyre regions.

the CPC and the SRTT. This can mostly be explained by the amount of rubber in the tread. Even though the total contribution of the tyre structure to the rolling resistance is very similar for all surfaces, there are some differences in which parts of the tyre contribute most. This is shown in Fig. 13 where the distribution of losses over the different elements in the WFE mesh is shown for the CPC tyre and the ISO and SD 11/16 surfaces. While the contribution of the bead, sidewall and shoulder areas is nearly identical, some differences are obtained for the tread region. For the ISO surface the losses originating from the solid and the shell elements in the tread region are nearly identical, see Fig. 13(a). For the SD 11/16 surface, in contrast, there is considerably less contribution from the shell elements, and more contribution from the solid elements, see Fig. 13(b). Expressed differently, for the ISO surface the tyre contributes more globally with a deformation of the whole belt/tread structure to the losses. For the rougher surface there is less global contribution from the tyre structure and more contribution from a local deformation of the tread rubber by the road surface asperities. This explains why the measured rolling resistance for the SD 11/16 surface is nearly identical for the SRTT and the CPC tyre as differences between the two tyre structures become less important.

The minimal variation of  $C_{r,tyre}$  for the different road surfaces implies that the variation of the rolling resistance for the different road surfaces is mainly explained by a variation of the losses originating in the small-scale contact deformation  $C_{r,tread}$ . This is confirmed by Fig. 12(a) where for the CPC tyre the small-scale contribution varies from negligible  $0.9 \cdot 10^{-4}$  for the ISO surface to  $0.825 \cdot 10^{-2}$  for the SD 11/16, which is nearly half of the overall  $C_r$  for this surface. Identical tendencies are visible for the other two tyres in Figures 12(b/c).

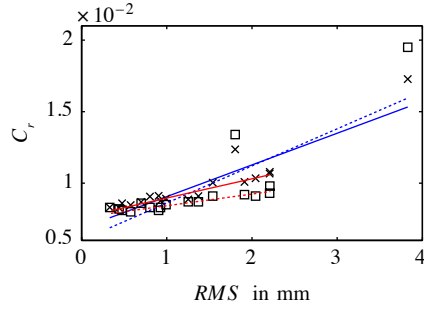
It can be concluded that there are two main mechanisms for the rolling resistance: firstly, there is the global deformation of the tyre structure due to the load. These losses vary only slightly with road surface texture and contribute with 50% to 100% to the overall losses. There is, however, a variation in which parts of the tyre structure contribute the most to these losses. Secondly, there are losses due to the small-scale deformation of the tread caused by the road surface asperities. These losses vary considerably with the surface profile; for smooth surfaces they are negligible whereas for very rough surfaces nearly 50% of the losses can be attributed to them.

In [17] a good correlation between  $C_r$  and  $RMS$  has been reported. For the data considered in the present study, this is mostly true as well, see Figures 14(a/b). The correlation is in the order of  $r \approx 0.82$  for the measurements and  $r \approx 0.91$  for the simulations if all road surfaces are considered.



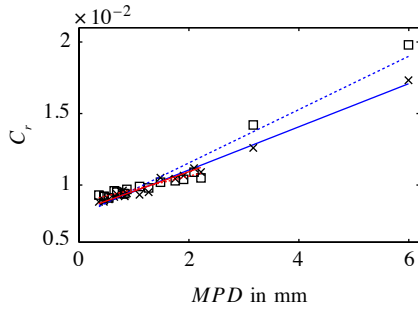
(a) *RMS* CPC:

fit sim. (all surf.)  $C_r = 0.0074 + 0.0021RMS$  ( $r = 0.91$ )  
 fit meas. (all surf.)  $C_r = 0.0073 + 0.0024RMS$  ( $r = 0.83$ )  
 fit sim. (excl. SD)  $C_r = 0.0082 + 0.0013RMS$  ( $r = 0.96$ )  
 fit meas. (excl. SD)  $C_r = 0.0088 + 0.0009RMS$  ( $r = 0.96$ )



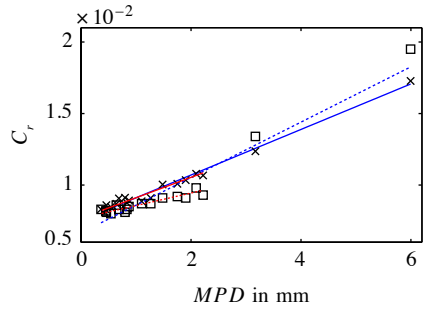
(b) *RMS* SRTT:

fit sim. (all surf.)  $C_r = 0.0069 + 0.0022RMS$  ( $r = 0.91$ )  
 fit meas. (all surf.)  $C_r = 0.0060 + 0.0026RMS$  ( $r = 0.81$ )  
 fit sim. (excl. SD)  $C_r = 0.0077 + 0.0013RMS$  ( $r = 0.96$ )  
 fit meas. (excl. SD)  $C_r = 0.0077 + 0.0008RMS$  ( $r = 0.93$ )



(c) *MPD* CPC:

fit sim. (all surf.)  $C_r = 0.0081 + 0.0015MPD$  ( $r = 0.99$ )  
 fit meas. (all surf.)  $C_r = 0.0079 + 0.0018MPD$  ( $r = 0.97$ )  
 fit sim. (excl. SD)  $C_r = 0.0082 + 0.0014MPD$  ( $r = 0.97$ )  
 fit meas. (excl. SD)  $C_r = 0.0088 + 0.0009MPD$  ( $r = 0.96$ )



(d) *MPD* SRTT:

fit sim. (all surf.)  $C_r = 0.0076 + 0.0016MPD$  ( $r = 0.99$ )  
 fit meas. (all surf.)  $C_r = 0.0066 + 0.0020MPD$  ( $r = 0.96$ )  
 fit sim. (excl. SD)  $C_r = 0.0077 + 0.0014MPD$  ( $r = 0.97$ )  
 fit meas. (excl. SD)  $C_r = 0.0077 + 0.0009MPD$  ( $r = 0.94$ )

Figure 14: Correlation between measured ( $\square$ ) and simulated ( $\times$ ) rolling resistance and (a/b) *RMS* and (c/d) *MPD*. (—) fit for simulation, (---) fit for measurement. Fit over all surfaces in blue, fit excluding the SD surfaces in red.

In [17] a better correlation was reported. This can be explained by the fact that in [17] only road surfaces with  $RMS < 2.2$  mm and  $C_r < 1.5 \cdot 10^{-2}$  have been considered. Limiting the analysis to the same *RMS* range as in [17], i.e. excluding the two SD surfaces from the fit, a better correlation for both measurements ( $r$  between 0.93 and 0.96) and simulations ( $r = 0.96$ ) is achieved. This does not necessarily indicate that the results for the rough SD surfaces are outliers, it might as well be a sign that the *RMS* is not a good predictor of rolling losses for rough surfaces.

A considerably better fit is achieved when  $C_r$  is plotted against the *MPD*, see Figures 14(c/d). The fit quality is between  $r = 0.94$  (measurements) and  $r = 0.99$  (simulations), indicating an excellent correlation between  $C_r$  and *MPD*, regardless of whether the SD surfaces are excluded from the fit or not. In Section 3 it was observed that when comparing *RMS* and *MPD* for the different road surfaces there is a variation in the ranking of the SD 5/8 surface, cf. Fig. 8. It can now be concluded that the road surface ranking based on the *MPD* is a more accurate descriptor

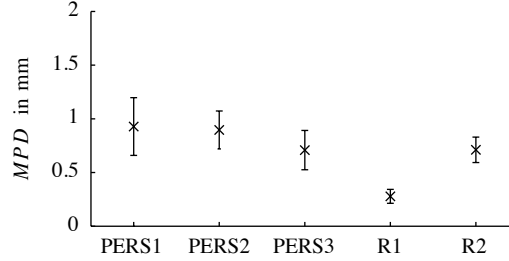


Figure 15: Average of the *MPD* for the rubberised surfaces. Average based on all measurement positions and all tracks. Errorbars indicate standard deviation. Note the difference in y-axis scaling compared to Fig. 8(b).

of the rolling resistance behaviour of the road surfaces than the *RMS*. Averaging over both tyres, and including all road surfaces, every millimetre increase in *MPD* raises the rolling resistance coefficient by circa  $0.16 \cdot 10^{-2}$  in the simulations and circa  $0.19 \cdot 10^{-2}$  in the measurements. This is in very good agreement with [48], where  $C_r \propto 0.0020 \cdot MPD$  was identified as giving excellent correlation. The lower slope of the simulation fit is mainly caused by the underestimation of the SD surfaces as is shown in Fig. 14.

Finally, it does not seem possible to establish a simple relation between the rolling resistance coefficient and the profile amplitude distributions shown in Fig. 9, or the average road surface spectra  $L_{Tx}$  in Fig. 10. This does not mean that no such connection exists; a deeper investigation of a possible relation was simply not within the scope of this study.

An important remark has to be made with respect to the good quantitative agreement between simulations and the measurements: this cannot be taken as an indicator that the proposed method is capable of giving a precise prediction of the rolling resistance for an individual tyre/road combination. This is partly due to simplifications in the model, e.g. the omission of friction, but mostly due to a large uncertainty in the rolling resistance measurements. In a round robin study [46] differences of up to 15% between different measurement methods were observed. In this respect the quantitative agreement between simulations and measurements might have been worse if another measurement system had been used in [26]. However, another conclusion in [46] is that the measurement systems determine nearly identical relative differences between different tyres or road surfaces. This is of great importance as it implies that the very accurate prediction of relative differences which is obtained from the simulations does not depend on the used measurement system. Simulated rankings of tread patterns or road surfaces with respect to the rolling resistance should accordingly be realistic.

## 5. Rolling resistance for rubberised surfaces

In addition to the traditional road surfaces described in Section 3 also rubberised road surfaces were measured in [25, 26]. Due to their special properties these are not included in the rolling resistance simulations presented in Section 4. Instead a concise evaluation of five of these surfaces, three poroelastic road surfaces (PERS) and two experimental surfaces (termed R1 and R2 in the following), and their properties follows here. Only data for the CPC tyre is presented as results the two other tyres are very similar.

In Fig. 15 the *MPD* is shown for all five road surfaces. Values are generally low, and for all cases apart from R1 the *MPD* is comparable to those of the TLA 2/6 and 4/8 surfaces in Fig. 8(b).

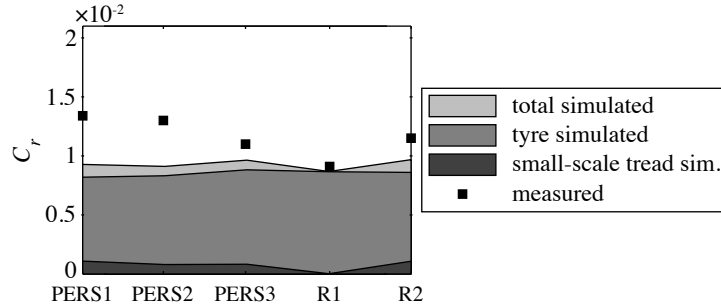


Figure 16: Rolling resistance for the CPC tyre on the rubberised surfaces.

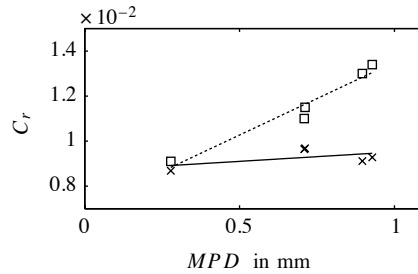


Figure 17: Correlation between measured ( $\square$ ) and simulated ( $\times$ ) rolling resistance and  $MPD$  for the CPC tyre and rubberised surfaces. (—) fit for simulation  $C_r = 0.0087 + 0.00084MPD$  ( $r = 0.53$ ), (---) fit for measurement  $C_r = 0.0071 + 0.0065MPD$  ( $r = 0.97$ ).

Surface R1 is extremely smooth, it has an  $MPD$  of 0.28 mm. For comparison, the ISO surface in Fig. 8(b) has an  $MPD$  of 0.36 mm.

The measured and calculated rolling resistances for the CPC tyre are shown in Fig. 16. For surface R1 a nearly perfect match between measurements and simulation is achieved. For all other surfaces, however, the simulations underestimate the measurements by up to 30%. The losses in the tyre structure are on a similar level as in Fig. 12. Accordingly, either the losses due to the small-scale tread deformation are too small for these surfaces, or there is another mechanism for rolling losses which is not covered by the simulations. A possible problem with the contact losses is that the contact formulation presented in Section 2.2, and with it the values for  $k_e$  and  $c_e$ , is based on the assumption of a completely rigid road. While this simplification is generally applicable for most traditional roads, it no longer holds for the rubberised surfaces. Yet, this does not fully explain why a good agreement between simulations and measurements is achieved for surface R1.

Recent studies have found rolling losses on poroelastic surfaces not to be higher than on comparable traditional road surfaces [49]. However, for the measurement results shown here,  $C_r$  values are obviously higher for the poroelastic surfaces. This is exemplified by comparing the correlation between the measured  $C_r$  and  $MPD$  in Fig. 17 with the one in Fig. 14(c). The slope of the fit for the rubberised surfaces is considerably higher than the one for the conventional surfaces. Therefore, for all  $MPD$  larger than approximately 0.18 mm the rolling resistance is (considerably) larger for the rubber surfaces. This might be explained by advancements in the construction of PERS between the time of the creation of the test sections for the AOT project and

the recent studies [49]. It is for example conceivable that friction or adhesion processes which can constitute additional rolling loss mechanisms are relevant for the three PERS considered here, but are of lesser importance for newer poroelastic surfaces.

## 6. Conclusions

A waveguide finite element tyre model and a non-linear tyre/road interaction model have been used to calculate the rolling resistance of a free rolling tyre on a real road surface. An effective way to handle the influence of the tread pattern has been introduced. Measured and simulated rolling resistances have been compared for combinations of three different tyres and 19 conventional road surfaces and five non-traditional rubberised road surfaces. The agreement between measured and simulated rolling resistance coefficients is very good for the traditional road surfaces. The influence of different tread patterns is adequately captured; some limitations compared to measurements on different tyres are given by the fact that only the different tread patterns but not the different tyre structures have been modelled. In the simulations the influence of the road surface texture on the rolling resistance is very similar to the measurements. With respect to the comparison between measurements and simulations it has to be pointed out that the overall level of quantitative agreement might depend on the used measurement technique. This does, however, not affect the faithful prediction of relative differences. Supporting recent findings in literature [48], the mean profile depth is identified to correlate very well with rolling resistance.

It was found that rolling resistance can be split into two parts: one part originating from the large-scale tyre structure deformations, and the other part arising from small-scale tread indentations. The contribution of the tyre structure to the overall rolling resistance is nearly identical for all road surfaces. However, variations of the distribution of losses between the belt package and the tread rubber could be observed, with the tread contributing more for rougher surfaces.

The losses due to small-scale tread deformations are highly texture depending and range from being 0 % to 25 % of the overall losses for smoother surfaces, and up to 50 % for the rough surface dressings. Summarising, it can be concluded that for smooth surfaces rolling resistance is mainly due to a global deformation of the tyre structure, whereas for rougher surfaces significant contributions are made by local deformations of the tread due to roughness asperities. The latter also leads to slightly less global deformation of the tyre, meaning that the tyre structure is of lesser importance for the rolling resistance on rougher road surfaces.

For the non-traditional rubberised surfaces the calculations could, with one exception, not accurately predict the measured rolling resistance. This is possibly related to modelling the road surface as rigid in the tyre/road interaction or a significant contribution of friction or adhesion mechanisms which are of lesser relevance for traditional road surfaces. A more precise assessment of possible reasons for the mismatch needs a broader set of data and should include simulations for newer rubberised surfaces which have been reported to have rolling resistance more equal to traditional surfaces.

Additional data might also be helpful for a further analysis of the results for traditional road surfaces: because of a lack of road texture scans so far only very few surfaces with an *MPD* > 2.5 mm (i.e. rougher surfaces) have been included in the analysis. While it is desirable for future work to include more surfaces, especially of “rougher” type, this might be difficult to realise as not only texture scans are needed, but also rolling resistance measurements which are comparable to those which have been used in this study.

It is conceivable that the results for both conventional and rubberised surfaces would benefit from a contact stiffness  $k$  which is scaled in relation to the actual road roughness profile. This will be a topic of future research.

In conclusion, the proposed method is very well suited for qualitative and quantitative studies of the rolling resistance of a free rolling tyre on traditional road surfaces. Due to its numerical efficiency, it is particularly useful for extended parameter studies, e.g. regarding road surface properties or tread pattern influence. For the present study 376 different cases could be calculated with reasonable numerical effort: on a 2012 workstation with six 3.2 GHz cores and 32 GB memory two cases could be solved in parallel in approximately two hours.

### Acknowledgements

The funding from the project *LeiStra3* (Leiser Straßenverkehr 3) under Grant 86.0079/2010, financed by the German Federal Ministry for Economic Affairs and Energy, and the German Federal Ministry of Transport and Digital Infrastructure, is gratefully acknowledged.

### References

- [1] J. Barrand, J. Bokar, Reducing tire rolling resistance to save fuel and lower emissions, *SAE International Journal of Passenger Cars – Mechanical Systems* 1 (2009) 9–17.
- [2] G. Fontaras, Z. Samaras, On the way to 130 g CO<sub>2</sub>/km—Estimating the future characteristics of the average European passenger car, *Energy Policy* 38 (2010) 1826–1833.
- [3] Tires and Passenger Vehicle Fuel Economy: Informing Consumers, Improving Performance, TRB Special Report 286, Transportation Research Board, 2006.
- [4] P.S. Pillai, Total tire energy loss comparison by the whole tire hysteresis and the rolling resistance methods, *Tire Science and Technology* 23 (1995) 256–265.
- [5] L.H. Yam, J. Shang, D.H. Guan, A.Q. Zhang, Study on tyre rolling resistance using experimental modal analysis, *International Journal of Vehicle Design* 30 (2002) 251–262.
- [6] D.S. Stutts, W. Soedel, A simplified dynamic model of the effect of internal damping on the rolling resistance in pneumatic tires, *Journal of Sound and Vibration* 155 (1992) 153–164.
- [7] S.J. Kim, A.R. Savkoor, The contact problem of in-plane rolling of tires on a flat road, *Vehicle System Dynamics* 27 (1997) 189–206.
- [8] A.J.P. Miège, A.A. Popov, Truck tyre modelling for rolling resistance calculations under a dynamic vertical load, *Proceedings of the Institution of Mechanical Engineers – Part D – Journal of Automobile Engineering* 219 (2005) 441–456.
- [9] H.C. Park, S.-K. Youn, T.S. Song, N.-J. Kim, Analysis of temperature distribution in a rolling tire due to strain energy dissipation, *Tire Science and Technology* 25 (1997) 214–228.
- [10] D.E. Hall, J.C. Moreland, Fundamentals of rolling resistance, *Rubber Chemistry and Technology* 74 (2001) 525–539.
- [11] K. Rao, R. Kumar, P. Bohara, A sensitivity analysis of design attributes and operating conditions on tyre operating temperatures and rolling resistance using finite element analysis, *Proceedings of the Institution of Mechanical Engineers – Part D – Journal of Automobile Engineering* 220 (2006) 501–517.
- [12] Y.-J. Lin, S.-J. Hwang, Temperature prediction of rolling tires by computer simulation, *Mathematics and Computers in Simulation* 67 (2004) 235–249.
- [13] J. Cho, H. Lee, W. Jeong, K. Jeong, K. Kim, Numerical estimation of rolling resistance and temperature distribution of 3-D periodic patterned tire, *International Journal of Solids and Structures* 50 (2013) 86–96.
- [14] P. Ghosh, A. Saha, R. Mukhopadhyay, Prediction of tyre rolling resistance using FEA, in: J. Busfield, A. Muhr (Eds.), *Constitutive Models for Rubber III*, Swets & Zeitlinger, Lisse, 2003.
- [15] J.R. Luchini, J.M. Peters, R.H. Arthur, Tire rolling loss computation with the finite element method, *Tire Science and Technology* 22 (1994) 206–222.
- [16] R. Ali, R. Dhillon, M. El-Gindy, F. Öjjer, I. Johansson, M. Trivedi, Prediction of rolling resistance and steering characteristics using finite element analysis truck tyre model, *International Journal of Vehicle Systems Modelling and Testing* 8 (2013) 179–201.

- [17] S. Boere, I. Lopez Arteaga, A. Kuijpers, H. Nijmeijer, Tyre/road interaction model for the prediction of road texture influence on rolling resistance, *International Journal of Vehicle Design* 65 (2014) 202–221.
- [18] M. Fraggstedt, Vibrations, damping and power dissipation in car tyres, PhD thesis, KTH Royal Institute of Sciences, Stockholm, 2008.
- [19] International Organization for Standardization ISO 18164:2005 Passenger car, truck, bus and motorcycle tyres — Methods of measuring rolling resistance, 2005.
- [20] C. Hoever, W. Kropp, A simulation-based parameter study of car tyre rolling losses and sound generation, in: *Euronoise Prague 2012*, 10–13 June 2012, pp. 926–931.
- [21] W. Kropp, Ein Modell zur Beschreibung des Rollgeräusches eines unprofilierten Gürtelreifens auf rauher Straßenoberfläche, PhD thesis, Fortschrittberichte VDI, Reihe 11: Schwingungstechnik, Nr. 166, 1992.
- [22] K. Larsson, W. Kropp, A high-frequency three-dimensional tyre model based on two coupled elastic layers, *Journal of Sound and Vibration* 253 (2002) 889–908.
- [23] F. Wullens, W. Kropp, A three-dimensional contact model for tyre/road interaction in rolling conditions, *Acta Acustica united with Acustica* 90 (2004) 702–711.
- [24] W. Kropp, P. Sabiniarz, H. Brick, T. Beckenbauer, On the sound radiation of a rolling tyre, *Journal of Sound and Vibration* 331 (2012) 1789–1805.
- [25] W. Schwanen, H.M. van Leeuwen, A.A.A. Peeters, G.J. van Blokland, H.F. Reinink, W. Kropp, Acoustic Optimization Tool — RE3: Measurement data Kloosterzande test track, Technical Report M+P.DWW.06.04.8, M+P – consulting engineers, 2007.
- [26] S. Boere, G.J. van Blokland, Influence of road surface properties on rolling resistance of car tyres, Technical Report M+P.DVS.08.17.1, M+P – consulting engineers, 2008.
- [27] D.J. O’Boy, A.P. Dowling, Tyre/road interaction noise — Numerical noise prediction of a patterned tyre on a rough road surface, *Journal of Sound and Vibration* 323 (2009) 270–291.
- [28] P. Kindt, P. Sas, W. Desmet, Development and validation of a three-dimensional ring-based structural tyre model, *Journal of Sound and Vibration* 326 (2009) 852–869.
- [29] C. Lecomte, W.R. Graham, M. Dale, A shell model for tyre belt vibrations, *Journal of Sound and Vibration* 329 (2010) 1717–1742.
- [30] M. Brinkmeier, U. Nackenhorst, S. Petersen, O. von Estorff, A finite element approach for the simulation of tire rolling noise, *Journal of Sound and Vibration* 309 (2008) 20–39.
- [31] C.-M. Nilsson, Waveguide finite elements applied on a car tyre, PhD thesis, KTH Royal Institute of Sciences, Stockholm, 2004.
- [32] Y. Waki, B.R. Mace, M.J. Brennan, Free and forced vibrations of a tyre using a wave/finite element approach, *Journal of Sound and Vibration* 323 (2009) 737–756.
- [33] P. Sabiniarz, W. Kropp, A waveguide finite element aided analysis of the wave field on a stationary tyre, not in contact with the ground, *Journal of Sound and Vibration* 329 (2010) 3041–3064.
- [34] S. Finnveden, M. Fraggstedt, Waveguide finite elements for curved structures, *Journal of Sound and Vibration* 312 (2008) 644–671.
- [35] K. Larsson, Modelling of dynamic contact — Exemplified on the tyre/road interaction, PhD thesis, Chalmers University of Technology, Gothenburg, 2002.
- [36] P.B.U. Andersson, W. Kropp, Time domain contact model for tyre/road interaction including nonlinear contact stiffness due to small-scale roughness, *Journal of Sound and Vibration* 318 (2008) 296–312.
- [37] P. Sabiniarz, Modelling the vibrations on a rolling tyre and their relation to exterior and interior noise, PhD thesis, Chalmers University of Technology, Gothenburg, 2011.
- [38] K.H. Hunt, F.R.E. Crossley, Coefficient of restitution interpreted as damping in vibroimpact, *Journal of Applied Mechanics* 42 (1975) 440–445.
- [39] G. Gilardi, I. Sharf, Literature survey of contact dynamics modelling, *Mechanism and Machine Theory* 37 (2002) 1213–1239.
- [40] K. Larsson, S. Barrelet, W. Kropp, The modelling of the dynamic behaviour of tyre tread blocks, *Applied Acoustics* 63 (2002) 659–677.
- [41] SPERoN acoustic optimization tool, <http://www.speron.net>, last visited 14/08/2014.
- [42] F. Wullens, W. Kropp, P. Jean, Quasi-3D versus 3D contact modelling for tyre/road interaction, in: *Internoise Prague 2004*, 22–25 August 2004.
- [43] International Organization for Standardization ISO 10844:2011 Acoustics – Specification of test tracks for measuring noise emitted by road vehicles and their tyres, 2011.
- [44] International Organization for Standardization ISO 13473-2:2002 Characterization of pavement texture by use of surface profiles — Part 2: Terminology and basic requirements related to pavement texture profile analysis, 2002.
- [45] International Organization for Standardization ISO/TS 13473-4:2008 Characterization of pavement texture by use of surface profiles — Part 4: Spectral analysis of surface profiles, 2008.
- [46] M.S. Roovers, D.F. de Graff, R.K.F. van Moppes, Round Robin Test Rolling Resistance / Energy Consumption,

- Technical Report DWW-2005-046, IPG, 2005.
- [47] A.N. Gent, J.D. Walter (Eds.), The pneumatic tire, U.S. Department of Transportation, National Highway Traffic Safety Administration, 2006.
  - [48] U. Sandberg, A. Bergiers, J.A. Ejsmont, L. Goubert, R. Karlsson, M. Zöllner, Road surface influence on tyre/road rolling resistance, Project Report MIRIAM SP1 04, 2011.
  - [49] J.A. Ejsmont, B. Świeczko Żurek, G. Ronowski, S. Taryma, Intermediate Report on Rolling Resistance, PER-SUADE Deliverable D.6.2, Technical University of Gdansk, 2014.